WPEDU-PR(17) 18435

A Zinovev et al.

Constitutive law for thermally-activated plasticity of recrystallized tungsten

Preprint of Paper to be submitted for publication in
Journal of Nuclear Materials

This work has been carried out within the framework of the EUROfusion Consortium and has received funding from the Euratom research and training programme 2014-2018 under grant agreement No 633053. The views and opinions expressed herein do not necessarily reflect those of the European Commission.

Constitutive law for thermally-activated plasticity of recrystallized tungsten

Aleksandr Zinovev[a,b,*], Dmitry Terentyev[a], Andrii Dubinko[a,c], Laurent Delannay[b]

[a] Institute for Nuclear Materials Science, SCK•CEN, Boeretang 200, 2400 Mol, Belgium

[b] iMMC, Université catholique de Louvain, Av. Georges Lemaître 4, 1348 Louvain-la-Neuve, Belgium

[c] Department of Applied Physics, Ghent University, St. Pietersnieuwstraat 41, 9000 Ghent, Belgium

*Corresponding author: tel.: +32 14 33 30 96, e-mail: aleksandr.zinovev@sckcen.be (Aleksandr Zinovev)

Keywords

Tungsten; constitutive equation; plasticity; deformation stage IV

Highlights

- Constitutive law for recrystallized W in the low temperature application window
- The effect of deformation stage IV is taken into account
- Model validation by means of finite element analysis

Abstract

A physically-based constitutive law relevant for ITER-specification tungsten grade in as-recrystallized state is proposed. The material demonstrates stages III and IV of the plastic deformation, in which hardening rate does not drop to zero with the increase of applied stress. Despite the classical Kocks-Mecking model, valid at stage III, the strain hardening asymptotically decreases resembling a hyperbolic function. The materials parameters are fitted by relying on tensile test data and by requiring that the strain and stress at the onset of diffuse necking (uniform elongation and ultimate tensile strength correspondingly) as well as the yield stress be reproduced. The model is then validated in the temperature range 300-600°C with the help of finite element analysis of tensile tests which confirms the reproducibility of the experimental engineering curves up to necking, beyond which the development of ductile

damage accelerates failure. This temperature range represents the low temperature application window for tungsten as divertor material in fusion reactor ITER.

1. Introduction

Emerging need to limit CO_2 emission as well as to enhance efficiency under operation of available electric power plants drives research towards high temperature applications [1], including nuclear energy domain. In a fusion power plant, energy must be extracted at extremely high temperatures and materials must demonstrate multi-functional capacity to serve as structural, armour or heat transfer component [2]. Given the high thermal conductivity, strength and melting point, refractory metals and in particular tungsten (W), are being considered as primary candidates. One of the critical problems in high temperature applications of refractory metals is mechanical performance in the low-temperature window, where these metals exhibit limited ductility due to relatively high ductile-to-brittle transition temperature (DBTT) [3]. Structural integrity of W implies its application above the DBTT i.e. above 300-400°C. However, in the fusion environment the DBTT will raise further because of the thermo-mechanical and energetic neutron loads as well as thermal cyclic fatigue and penetration of plasma components [4]. Understanding of the elementary mechanisms driving plastic deformation, stress concentration and eventual failure is therefore an important direction of current research carried out by both experimental and theoretical/computational communities.

Only a few previous works have reported tensile tests involving significant ductility of ITER relevant tungsten grades: the grade labelled as M184 (in the as-recrystallized state after heavy deformation) [5] and labelled as IGP (standing for "ITER grade Plansee") [6]. Zhu et al. [7] applied Johnson-Cook model to characterize the work hardening of commercially pure tungsten fabricated by AT&M in the temperature range 20-700°C. Wang et al. [8] reviewed the applicability of six constitutive equations based on Arrhenius, Johnson–Cook, modified Johnson–Cook, Zerilli–Armstrong, modified Zerilli–Armstrong, and Khan–Huang–Liang models to the description of hot deformation of powder metallurgy tungsten. Since low temperature deformation of W (i.e. above $0.15T_m$, where T_m is the melting point), just as in other BCC metals, is primarily controlled by the motion of dislocations, their multiplication and interaction with grain boundaries (GB) [9], several previous studies have used the Kocks-Mecking equation based on thermally-activated dislocation-dislocation interaction to describe work hardening of double-forged commercially pure tungsten [10] and K-doped tungsten [11] in the temperature range 500-2000°C both fabricated by Plansee AG.

Here we extend the study initiated by Terentyev et al [10] and consider larger strain. Experiments presented next show that a saturating hardening law, such as the original Kocks-Mecking law, is not convenient for the description of deformation hardening of as-recrystallized IGP tungsten. To improve the existing model, the effect of deformation stage IV must be considered. Deformation stage IV in FCC and BCC metals and alloys was revealed in torsion tests which postpone the development of deformation instability and allow attaining large strain [12, 13]. Instead of saturating at the end of stage III, the true stress maintained basically linear increase within a wide strain range (up to ~10 in Fe, and ~5 in Ni at 293 K) [13].

The occurrence of stage IV hardening is often attributed to dislocation storage in the form of a cellular structure inside individual grains. Several approaches have been proposed to understand the cellular structure formation and its impact on the subsequent stress-strain evolution [14-16]. Although the dislocation density in the cell interiors does indeed saturate with strain, in accordance with the Kocks-Mecking law, the dislocation density in the cell walls keeps growing and contributing to hardening. Importantly, most of those works dealt with FCC metals due to their superior capacity for plastic deformation as compared to BCC metals. However, the cellular structure was observed in BCC tungsten deformed in compression in the range from room temperature up to 600°C by Chiem [17] and Dubinko [18]. Stephens [19] investigated the microstructure of single crystal tungsten (and dilute W-based alloys) in a wide temperature range from 150 K ($0.04T_m$) up to 590 K ($0.16T_m$) under compressive deformation. Kocks-Mecking models, modified to account for cellular structures, were successfully used to describe deformation stage IV in FCC metals with the help of a second state variable associated with lattice incompatibility [20] as well as in BCC metals and alloys including pure tungsten [21] and Ta-10W alloy by introduction of a separate dislocation substructure density [22].

Up to our best knowledge, there is no model addressing the behaviour of ITER specification W based on thermally-activated dislocation slip, suitable to describe the effect of temperature and strain rate on ductility. The purpose of the present computational study is to incorporate the above noted important experimental observations and develop a constitutive law for plastic deformation, accounting for both experimental and theoretical studies [10, 23]. The ultimate goal is thus to develop an efficient set of constitutive equations suitable for application by finite element analysis (FEA) to upscale and investigate the mechanical response of tungsten subjected to complex thermo-mechanical loads, e.g. cyclic heat loads resulting from the plasma instability during operation of fusion devices. Although a single heat cycle leads to a fraction of percent of plastic strain, the damage in tungsten components develops after a number of such cycles. Consequently, plastic strain, being irreversible, accumulates up to a considerable value, leading

to significant strain hardening, which is accounted by the present model. We believe that the ideally-plastic constitutive law is less applicable for the simulation of this physical process, being, however, a decent approximation in simulations of just a few heat cycles.

The work is arranged in the following way. We first present recent experimental tensile test data for commercial tungsten, which will be used as a guideline for the validation of the model. Then the model is presented and we demonstrate that the results of calculations (including FEA) tend to agree with experimental data.

2. Experimental data

Tensile tests were performed at SCK-CEN, Belgium, in the temperature range 300-600°C and strain rates $6 \cdot 10^{-5} ... 6 \cdot 10^{-3}$ 1/s on commercially pure W produced by Plansee AG according to the ITER specification [24] (henceforth "IGP W"). Figure 1a presents the true stress - true strain data for the recrystallized material obtained by annealing at 1600°C for one hour [6]. The terms “as-annealed” and “as-recrystallized” are used interchangeably in the present text. The material deformed at high temperature demonstrates increased ductility (uniform elongation up to 30%) and a constant hardening rate (in terms of true stress) at large strain, which corresponds to stage IV. The hardening rate vs. true stress is shown in Figure 1b and it confirms that stage IV is pronounced at 500°C and above.

The material deformed below 500°C reached comparatively low fracture strain and, what is more important, did not undergo necking and ductile failure, thus being not suitable for model identification based on the ultimate tensile strength (UTS) and uniform elongation (UE). Nevertheless, the yield stress and initial hardening were used for the model validation.

The precise yield stress values and the engineering stress-strain curves extending beyond the onset of necking are reported in Section 4, together with the model predictions.

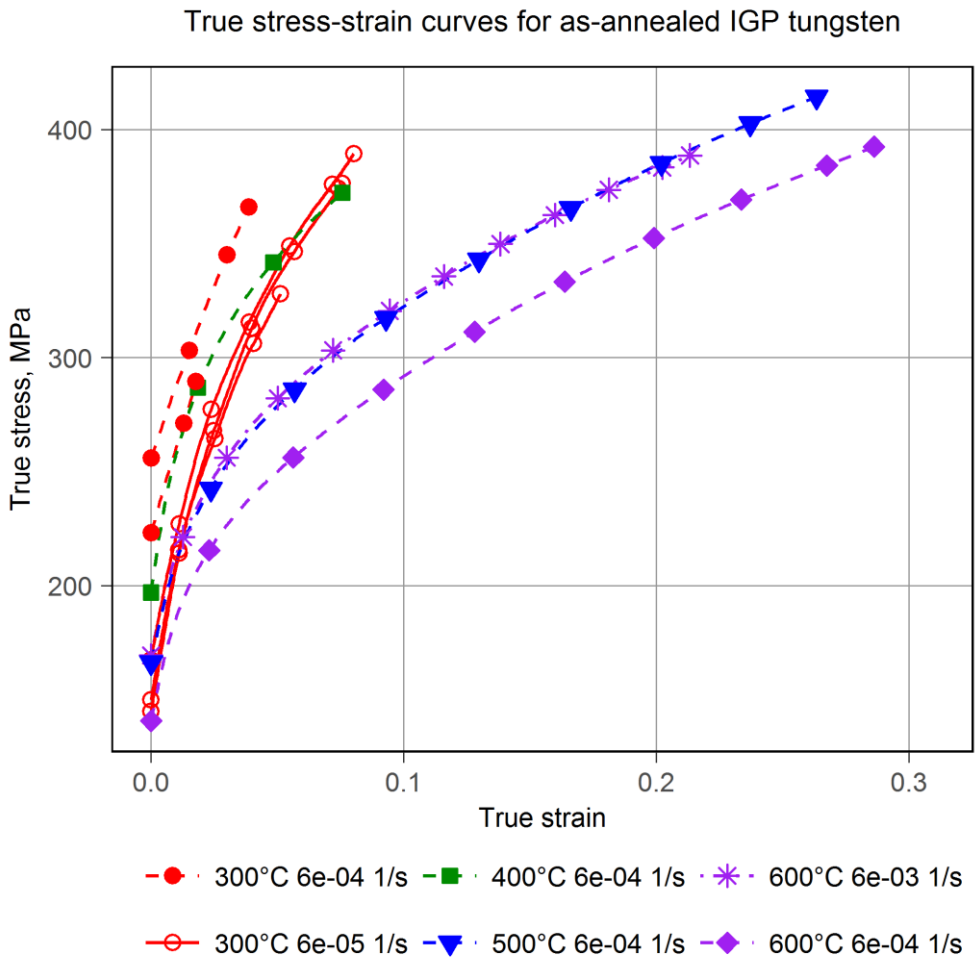
True stress-strain curves for as-annealed IGP tungsten
True stress, MPa
400
300
200
0.0
0.1
0.2
0.3
True strain
300°C 6e-04 1/s
400°C 6e-04 1/s
600°C 6e-03 1/s
300°C 6e-05 1/s
500°C 6e-04 1/s
600°C 6e-04 1/s

a)

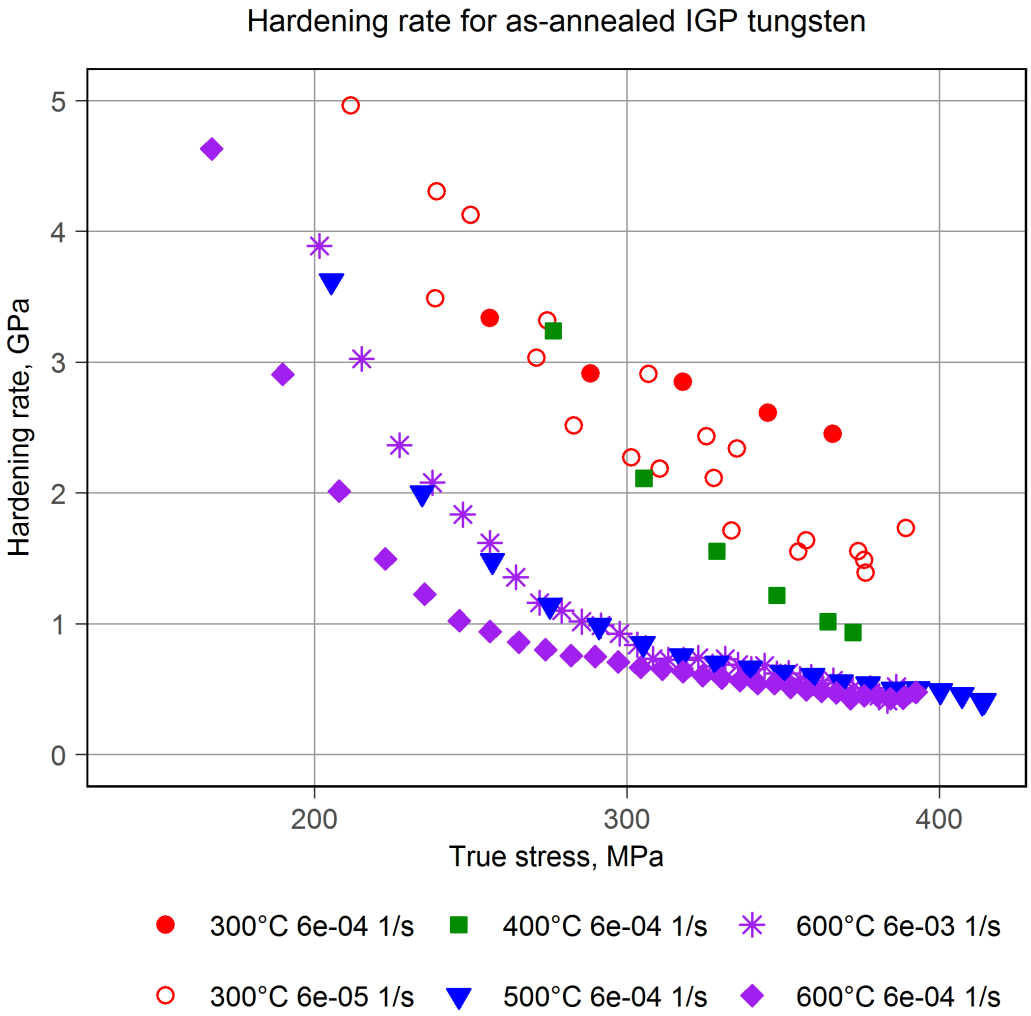

b)

Figure 1. a) Experimental true stress-strain curves and b) hardening rate derived from them for as-annealed IGP tungsten.

3. Model description

The initial yield stress σ_0 depends on temperature T and strain rate $\dot{\varepsilon}$ according to a phenomenological formula [22] adapted by adding a constant term S_0, to account for non-zero lattice friction stress at high temperature in BCC metals:

$$\sigma_0 = S\exp(BT)\left(K\ln\frac{\dot{\varepsilon}}{\dot{\varepsilon}_1}+L\right)+S_0 \qquad (1)$$

Strain hardening is described by adding to the common saturating Voce law [25] (representative of Stage III) a linear hardening term corresponding to Stage IV. For mathematical convenience, linear hardening is effective already at the onset of plasticity but its contribution becomes predominant only after attaining large strain, when the first term saturates:

$$\sigma_{Voce} = \sigma_{sat} + \left(\sigma_0 - \sigma_{sat}\right)\exp\left(-\frac{\varepsilon}{\varepsilon_0}\right) + H_{IV}\varepsilon \tag{2}$$

where σ_0 is the yield stress, σ_{sat} is the saturation value of Stage III hardening, ε is the accumulated plastic strain and ε_0 and H_{IV} are material parameters related to the initial and the final hardening rates, respectively.

The hardening parameters depend on strain rate and temperature. They are computed by considering Taylor hardening [26] which assumes that strength increases proportionally to the square root of the dislocation densityρ. If ρ_0 denotes the initial dislocation density, then:

$$\sigma = A\left(\sqrt{\rho} - \sqrt{\rho_0}\right) + \sigma_0 \tag{3}$$

The parameter *A* defines the strength due to dislocation interactions and it is assumed to vary linearly with temperature: $A=A_0+A_sT$.

The dislocation density is updated based on the Kocks-Mecking equation [26] assuming that dislocation storage and dislocation annihilation evolve as a function of $\sqrt{\rho}$ and ρ, respectively:

$$\dot{\rho} = M\dot{\varepsilon}\left(k_1\sqrt{\rho} - k_2\rho\right) \tag{4}$$

Here M is the Taylor factor, set equal to 2.5. Saturation occurs when the rate of dislocation multiplication (due to the dislocation-dislocation pinning) is balanced by recovery occurring via dislocation-dislocation annihilation and dislocation-GB interaction. These two processes are effectively parameterized by introducing coefficients: k_1 and k_2. Integration of Eq. (4) leads to the following expression for dislocation density as a function of the accumulated plastic strain:

$$\rho = \left(\frac{\sqrt{\rho_0} - \frac{k_1}{k_2}}{\exp\left(0.5Mk_2\varepsilon\right)} + \frac{k_1}{k_2}\right)^2 \tag{5}$$

If we combine the latter with Eq. (3), the saturating term of Eq. (2) (i.e. adapted Voce law) is recovered with

$$\sigma_{sat} = A\left(\frac{k_1}{k_2} - \sqrt{\rho_0}\right) + \sigma_0 \tag{6}$$

and

$$\varepsilon_0 = \frac{2}{Mk_2} \tag{7}$$

Inspired from the work of Prinz et al. [14] who consider a cellular dislocation structure in which the cell walls have non-saturating dislocation density, we add a term to Eq. (5) in order to let the total dislocation density increase beyond the saturation value $\left(\frac{k_1}{k_2}\right)^2$ at large strain, thus accounting for deformation stage IV:

$$\rho = \left(\frac{\sqrt{\rho_0} - \frac{k_1}{k_2}}{\exp\left(0.5Mk_2\varepsilon\right)} + \frac{k_1}{k_2} + H_{KM}\varepsilon \right)^2 \tag{8}$$

Then stress-strain relationship becomes:

$$\sigma = A\left(\frac{\sqrt{\rho_0} - \frac{k_1}{k_2}}{\exp\left(0.5Mk_2\varepsilon\right)} + \frac{k_1}{k_2} + H_{KM}\varepsilon - \sqrt{\rho_0} \right) + \sigma_0 \tag{9}$$

By matching Eqs. (2) and (9) we find corresponding parameters.

$$k_1 = \frac{2\left(\sigma_{sat} - \sigma_0 + A\sqrt{\rho_0}\right)}{AM\varepsilon_0} \tag{10a-b}$$
$$H_{IV} = AH_{KM}$$

As it is proposed in [10], k_1 is constant whereas k_2 accounts for the fact that dislocation recovery is a thermally activated process, following the equation adopted from the work of Beyerlein and Tomé [27].

$$k_2 = C_1\left(1 - C_2 T \ln\left(\frac{\dot{\varepsilon}}{\dot{\varepsilon}_0}\right)\right) \tag{11}$$

Here C_1, C_2 and $\dot{\varepsilon}_0$ are constants.

The model is implemented in the form of a UHARD, a user-defined subroutine for Abaqus, where the effect of both temperature and strain rate is accounted for. Thus sample regions experiencing different strain rates would harden in different manners, following the model equations.4. Results and discussion

The developed model was fitted to obtain the best single set of parameters to describe plastic deformation in terms of strain hardening behaviour in the temperature range 300-600°C.

First, Eq. (1) was fitted to achieve the best prediction of the experimentally measured yield stress, which is shown in Figure 2. The corresponding parameters of the equation are listed in Table 1 and used in the model.

Table 1. Parameters needed to calculate yield stress.

S	B	K	L	$\dot{\varepsilon}_1$	S_0
1268.4MPa	-3.6e-3 1/K	0.23	-0.518	1.22e-06 1/s	90.6MPa

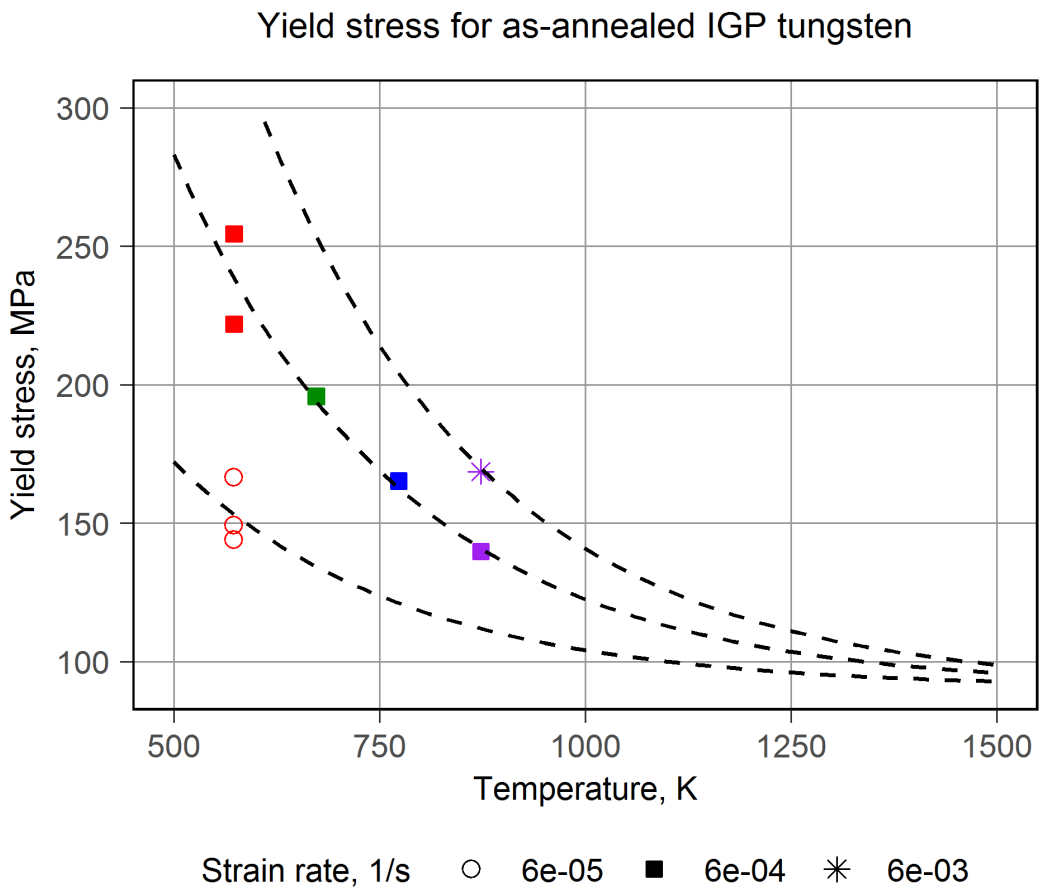

Figure 2. Yield stress for as-recrystallized IGP W. Symbols represent experimental data, and dotted lines highlight the evolution with temperature at a fixed strain rate.

The rest parameters were determined by ensuring that the model produces valid predictions of the onset of diffuse necking. According to the Considère criterion [28], the onset of diffuse necking during uniaxial tension occurs in the moment when the continuously decreasing hardening rate θ becomes equal to true stress σ in the specimen. The Considère criterion is traditionally obtained from solid mechanics considerations, but recently it was reported to also follow from intrinsic evolution laws (e.g. Kocks-Mecking) for the governing internal variable – the total dislocation density [29]. It is to be noted that the Considère criterion governs the initiation of necking irrespective of sample geometry. Although the total elongation of a tensile

sample and the post-necking region of a stress-strain curve may indeed depend on sample geometry (smaller total elongation is usually demonstrated by testing longer samples) [30], but both are out of the scope of the present study. Hence the present model is able to predict UE and UTS for samples with other geometries. However, the experiments were only performed on miniaturized samples of the same size, thus the validation of this statement is not deemed possible at the moment.

The evolution of hardening rate with strain can be derived from Eq. (9):

$$\theta = A\left(H_{KM} + \frac{0.5 \cdot Mk_2 \left(\frac{k_1}{k_2} - \sqrt{\rho_0} \right)}{\exp\left(0.5 \cdot Mk_2 \varepsilon\right)} \right) \tag{12}$$

The diffuse necking condition may be identified implicitly with the help of a fixed-point algorithm. The model parameters were fitted in such a way to reproduce both UE and UTS measured experimentally at different temperatures and strain rates. Only three true stress-strain curves which demonstrated necking (i.e. the tests performed at 500 and 600°C), were used to this end. R-coding and the Levenberg-Marquardt algorithm allowed solving the non-linear least squares problem [31, 32]. Due to an excess number of degrees of freedom, three parameters had to be fixed and were thus adopted from the literature, namely from the previous work by our team, devoted to a Kocks-Mecking like model of double-forged W fabricated by Plansee AG [10]. While the parameters k_1 and $\dot{\varepsilon}_0$, having equal meaning in the two models, were adopted directly, the match between Eq. (11) in the present paper and Eq. (9) in [10] allowed us to calculate C_1 as

$$C_1 = \frac{k_1 \chi b}{g} \tag{13}$$

where χ is an interaction parameter, b is Burgers vector and g is the normalized activation energy [10].

Table 2 indicates which parameters were fitted by solving the least squares problem and which ones were adopted from [10]. The initial dislocation density ρ_0 measured in as-recrystallized IGP W with the help of TEM was found to be 10^{11} m^{-2}.

Table 2.The fitted parameters.

Parameter	Definition	Value	Comment
ρ_0	Initial dislocation density	10^{11}m^{-2}	Measured
k_1	Kocks-Mecking parameter	$4.80\cdot10^{8}$m^{-1}	Adopted
C_1	For calculation of k_2	$4.20\cdot10^{-5}$	Adopted
C_2	For calculation of k_2	20.75 K^{-1}	Fitted
$\dot{\varepsilon}_0$	For calculation of k_2	10^{7} s^{-1}	Adopted
H_{KM}	Coefficient at the linear term	$7.68\cdot10^{7}$ m^{-1}	Fitted
A_0	For calculation of A	$7.64\cdot10^{-6}$MPa·m^{-1}	Fitted
A_s	For calculation of A	$-3.2\cdot10^{-9}$MPa·m^{-1}·K^{-1}	Fitted

The values of A and k_2 calculated for a set of temperatures are listed in Table 3 for illustrative purpose. We can see that the strength of dislocation-dislocation interaction decreases with temperature, while the dislocation annihilation, expressed by k_2, becomes more significant at higher temperatures.

Table 3. Values of dislocation-dislocation interaction parameter and the Kocks-Mecking parameter k_2 obtained from the fit.

T, °C	300	400	500	600
A, MPa·m^{-1}	$5.8\cdot10^{-6}$	$5.5\cdot10^{-6}$	$5.2\cdot10^{-6}$	$4.8\cdot10^{-6}$
k_2 (for $6\cdot10^{-4}$s^{-1})	11.8	13.8	15.9	17.9

Figure 3 shows both experimental (solid) and modelled (dashed) true stress-strain curves for IGP W deformed at different strain rates and temperatures. Only the three curves shown on the right correspond to tensile tests during which necking was observed and were used for the model fitting. The stress-strain curves calculated for 300°C and 400°C are plotted on the left along with the corresponding experimental ones, confirming a fair prediction of the yield stress and the initial hardening also in lower temperature range.

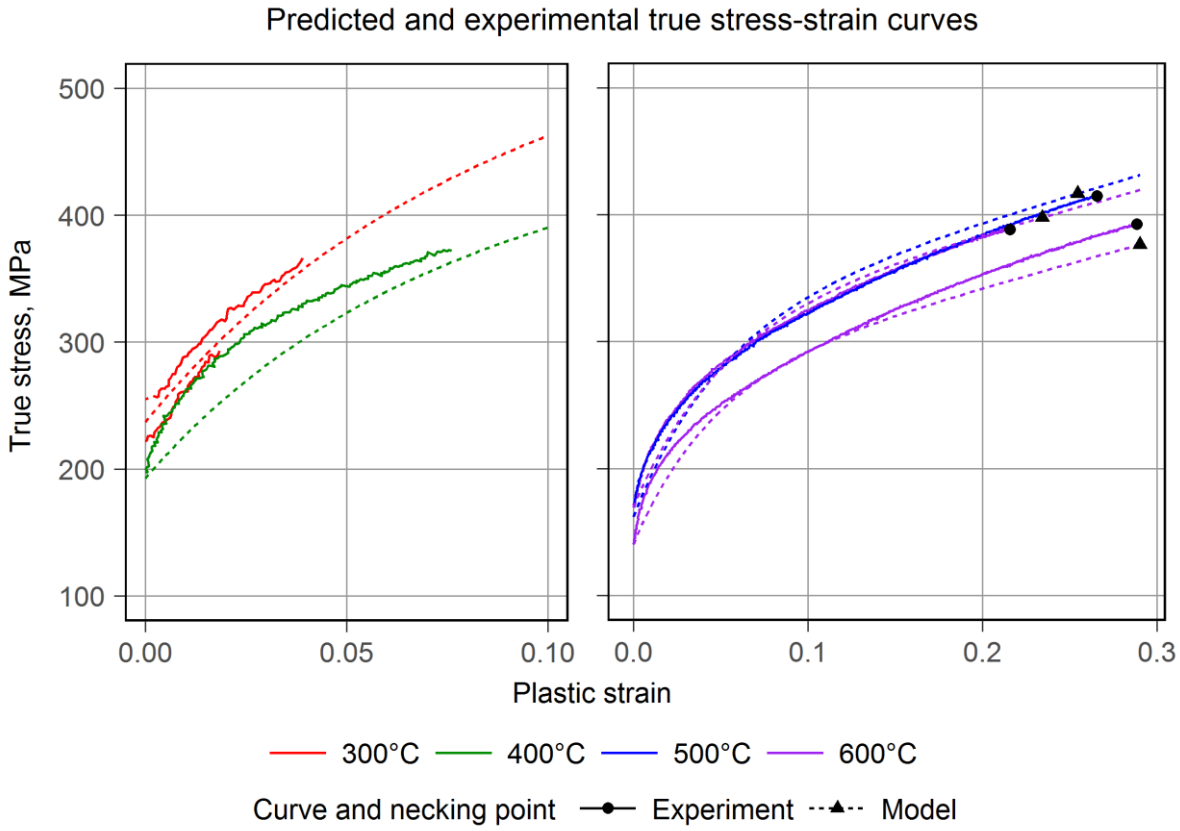

Figure 3.Experimental and fitted stress-strain curves for as-annealed IGP tungsten.

Due to the lack of IGP grade, interruptive tensile tests at 600°C and consequent TEM examination [18] have been performed on double-forged W grade samples (provided by Plansee AG) in the as-recrystallized state in order to investigate the microstructure evolution during plastic deformation. A Kocks-Mecking-like model of this tungsten grade was reported in the previous publication [10]. Interestingly, annealing of both grades (double-forged from the previous paper and IGP from the present one) under the same conditions leads to various dislocation density and grain size in the as-recrystallized state.

The presence of a cellular dislocation structure, which is responsible for Stage IV hardening [33], has been confirmed by the TEM examination. Figure 4 demonstrates that samples deformed up to 20% contain dislocation tangles (precursor of the dislocation walls) and those deformed up to 28% show the formation of cells, thus resulting in grain refinement [18]. Figure 5 provides a comparison between experimentally measured dislocation density and the prediction of the present model, revealing that the model overestimates the dislocation density. The initial dislocation density used in this particular calculation was assumed to be equal to $5 \cdot 10^{12}$ m^{-2}, i.e. the value measured experimentally in the double-forged tungsten, for which the interruptive tests were performed. [10]. It should, however, be noted that the experimental measurements excluded the dislocation density in the cell walls, which was considered as a pre-cursor of low angle GB.

This contributes to the discrepancy between our model results and the experimental data. More adequate assessment of the model will require additional TEM examination, which will be performed in the future, focussing on the dislocation density measurement in the regions adjacent to grain boundaries and determining their contribution to the total dislocation density.

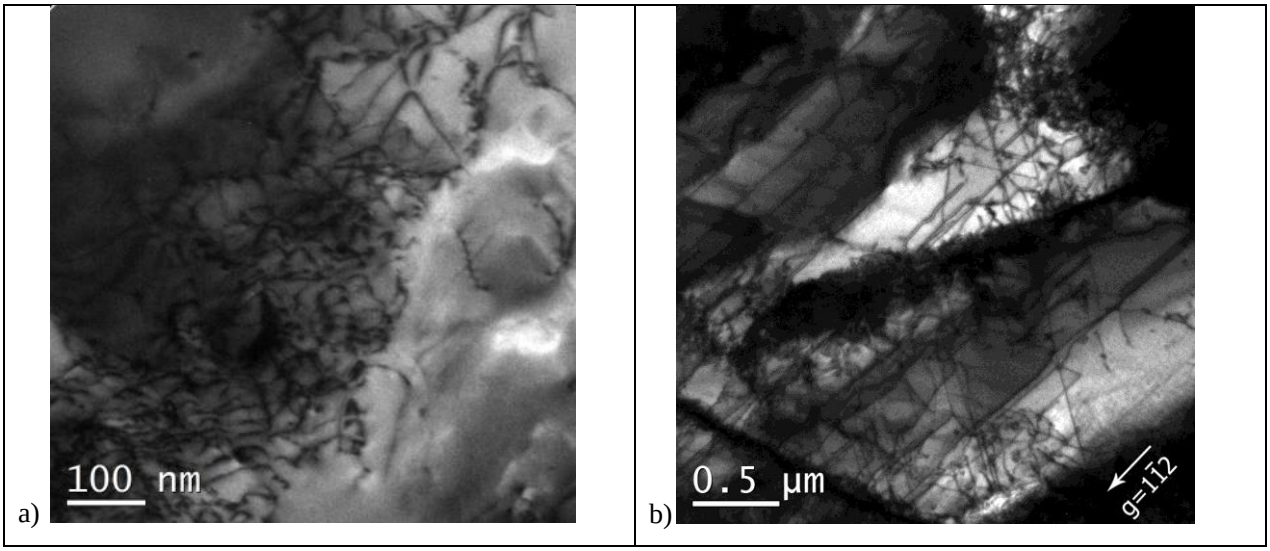

Figure 4. TEM micrographs showing dislocation tangles (a) and dislocation cells (b), probed by TEM at 20% (a) and 28%(b) of plastic strain. The grain refinement was observed in the tests done at 500°C and 600°C, and it occurred typically after 20% plastic strain.

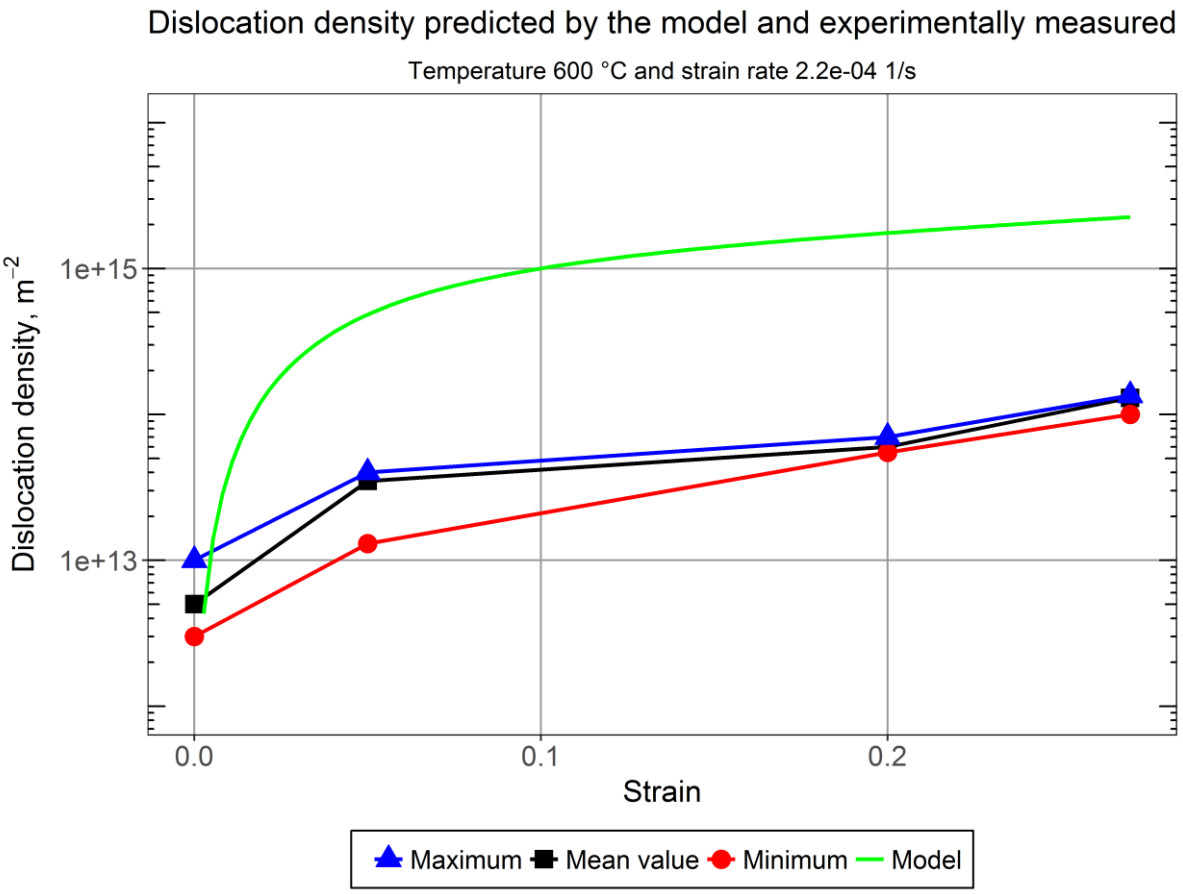

Figure 5.Dislocation density experimentally measured and predicted by the model.

In order to validate the model at strain at and a little beyond the onset of diffuse necking, we have performed displacement-controlled FE simulations of tensile tests with the help of the commercial software Abaqus 6.14-1. The sample geometry shown in Figure 6 represented the experimental specimen with a gauge length 5.2 mm and cross-section dimensions 1.6x1.8 mm^2. The sample was meshed into about 3100 second-order tetrahedral elements varying in size from 0.2 mm in the gauge middle area to 2.0 mm in the grips with the help of Gmsh software [34].

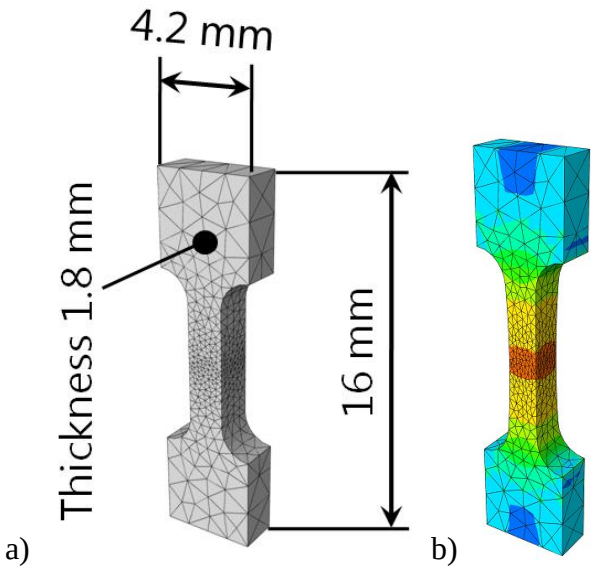

Figure 6. A tensile sample used in FE analysis at 600 C, a) in the non-deformed state; b) in the moment of necking. Colour represents von Mises stress, ranging from 0 (blue in the grips) to 400 MPa (red in the centre).

An example of von Mises stress distribution in the sample is presented in Figure 6b. The snapshot was taken at the initiation of plastic instability, when stress becomes nonuniform in the specimen gauge.

Figure 7 shows the engineering stress-strain curves obtained in experiments (solid) and in the simulations (dashed), they are grouped by test temperature and strain rate. We can see fair coincidence between them up to the neck formation, shortly after which the model tends to overestimate strength and fracture strain. The latter is most probably due to ductile damage accumulation.

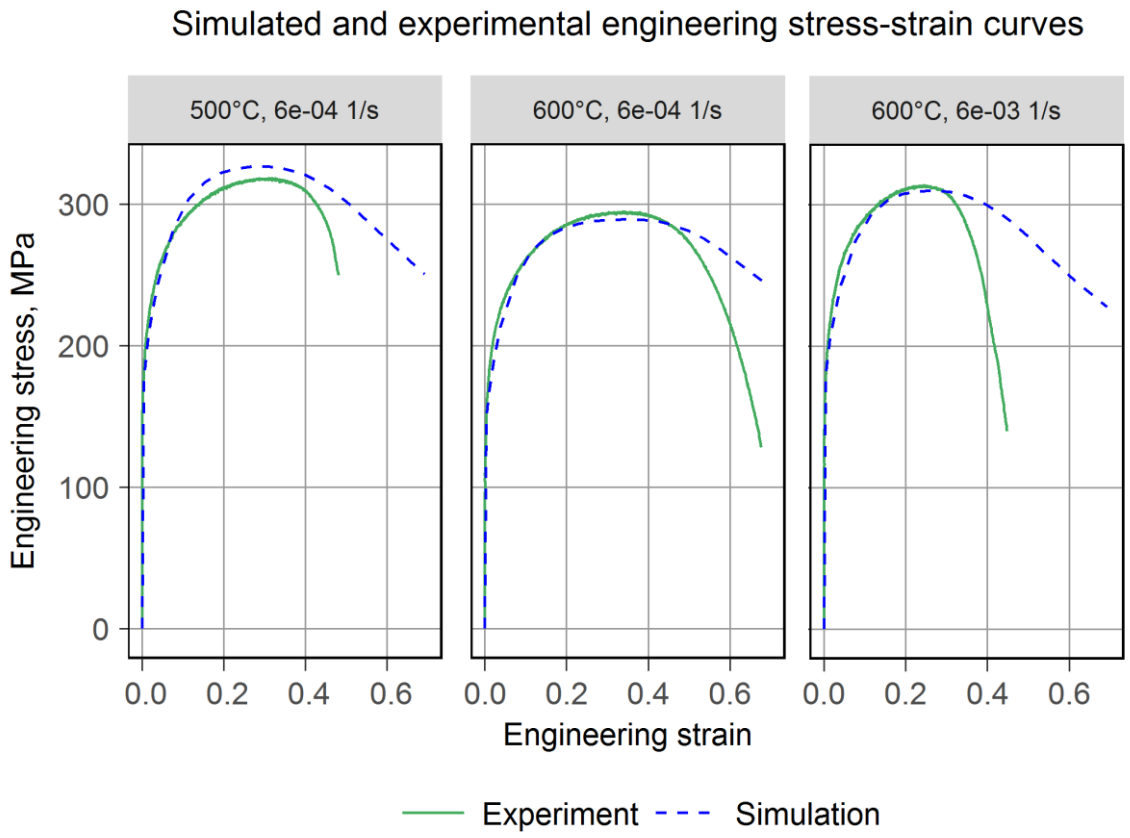

Figure 7.Experimental and simulated engineering stress-strain curves for as-recrystallized IGP tungsten.

The applicability of the model to the simulations of thermal loads relevant to ITER can be justified as follows. Due to the lack of data on tensile tests of as-recrystallized tungsten provided by Plansee AG, we have to use another grade as an example. Mechanical tests of W in a wide strain rate range performed by compression (10^{-3}…10^{0} 1/s), experiments on a compression Kolsky bar (10^{3}…10^{4} 1/s) and pressure-shear plate impact tests (10^{4}…10^{5} 1/s) are reported [35]. The studied material was obtained in the form of an extruded rod from Teledyne Firth-Sterling by the Army Research Laboratory, USA. The stress-strain curves for as-recrystallized W from, obtained at room temperature in the wide strain rate range (10^{-3}…10^{4} 1/s) by various test methods demonstrated consistent behaviour. Thus, in our opinion, plasticity of W can be described by the same set of equations up to a strain rate of ~10^{4} 1/s, which includes the strain rates relevant for the ELM-caused dilatation of W, ~8 1/s according to Ref. [5].

5. Conclusions

The present work includes a theoretical study of the plastic deformation of commercially pure W including stage IV. In particular, we have developed a macroscopic isotropic constitutive model accounting for the effect of temperature and strain rate on dislocation storage and the resulting hardening.

Deformation-induced grain refinement due to the build up of dislocation walls and cells has been confirmed by TEM investigations and it is assumed to lead to contribute to Stage IV hardening.

The study relies also on a direct experimental validation of the evolution of dislocation density and work-hardening rate at different stages of plastic deformation and different temperatures. The study is limited in the temperature range of 300-600°C which represents the low temperature application window for tungsten as divertor material in fusion reactor ITER, and thus being the most important from the view point of structural integrity.

At this point, we demonstrated that the currently proposed and simplified (as compared to full detail crystal plasticity) model is suitable to accurately predict the stress-strain behaviour in a large diapason of plastic strain for the commercial tungsten grade of ITER specification in the recrystallized state. The model is computationally efficient and it utilizes a physically-based approach which can be extended to account for the lattice defects induced by neutron irradiation and transmutation, since neutron damage and rhenium precipitation are other important limiting factors under fusion [36, 37].

The next important step is to push the model to treat W with the forged microstructure which exhibits a pronounced texture and elongated grains with multiple small sub-grains and initially high dislocation density.

Acknowledgements

This work has been carried out within the framework of the EUROfusion Consortium. Funding received from the Euratom research and training programme 2014-2018 (grant agreement No 633053). The views and opinions expressed herein do not necessarily reflect those of the European Commission. LD is mandated by the FNRS.

References

[1] S.J. Zinkle, J.T. Busby, Structural materials for fission & fusion energy, Materials today, 12 (2009) 12-19.
[2] S.J. Zinkle, Advanced materials for fusion technology, Fusion Engineering and Design, 74 (2005) 31-40.
[3] R.H. Titran, J.R. Stephens, D.W. Petrasek, Refractory-Metal Alloys and Composites for Space Nuclear-Power Systems, Jom-J Min Met Mat S, 40 (1988) A63-A63.
[4] G. Pintsuk, Tungsten as plasma facing material, Comprehensive Nuclear Materials, 4 (2012) 551-581.
[5] I. Uytdenhouwen, Degradation of first wall materials under ITER relevant loading conditions, PhD thesis, in: Faculteit Ingenieurswetenschappen, Universiteit Gent, 2011.

[6] M. Wirtz, J. Linke, T. Loewenhoff, G. Pintsuk, I. Uytdenhouwen, Thermal shock tests to qualify different tungsten grades as plasma facing material, Physica Scripta, T167 (2016) 014015.
[7] C.C. Zhu, Y.T. Song, X.B. Peng, Y.P. Wei, X. Mao, W.X. Li, X.Y. Qian, The dynamical mechanical properties of tungsten under compression at working temperature range of divertors, Journal of Nuclear Materials, 469 (2016) 120-124.
[8] J. Wang, G. Zhao, L. Chen, J. Li, A comparative study of several constitutive models for powder metallurgy tungsten at elevated temperature, Materials and Design, 90 (2016) 91-100.
[9] A. Giannattasio, Z. Yao, E. Tarleton, S.G. Roberts, Brittle–ductile transitions in polycrystalline tungsten, Philosophical Magazine, 90 (2010) 3947-3959.
[10] D. Terentyev, X. Xiao, A. Dubinko, A. Bakaeva, H. Duan, Dislocation-mediated strain hardening in tungsten: Thermo-mechanical plasticity theory and experimental validation, Journal of the Mechanics and Physics of Solids, 85 (2015) 1-15.
[11] H. Sheng, I. Uytdenhouwen, G. Van Oost, J. Vleugels, Mechanical properties and microstructural characterizations of potassium doped tungsten, Nuclear Engineering and Design, 246 (2012) 198-202.
[12] I. Kovács, The mechanism of the work-hardening in F.C.C. metals, Acta Metallurgica, 15 (1967) 1731-1736.
[13] P. Les, H.P. Stüwe, M. Zehetbauer, Hardening and strain rate sensitivity in stage IV of deformation in f.c.c. and b.c.c. metals, Materials Science and Engineering: A, 234-236 (1997) 453-455.
[14] F.B. Prinz, A.S. Argon, The Evolution of Plastic Resistance in Large Strain Plastic Flow of Single Phase Subgrain Forming Metals, Acta Metallurgica et Materialia, 32 (1984) 1021-1028.
[15] A.S. Argon, P. Haasen, A New Mechanism of Work Hardening in the Late Stages of Large Strain Plastic Flow in F.C.C. and Diamond Cubic Crystals, Acta metallurgica et materialia, 41 (1993) 3289-3306.
[16] Y. Estrin, L.S. Tóth, A. Molinari, Y. Bréchet, A dislocation-based model for all hardening stages in large strain deformation, Acta Materialia, 46 (1998) 5509-5522.
[17] C.Y. Chiem, W.S. Lee, The influence of dynamic shear loading on plastic deformation and microstructure of tungsten single crystals, Materials Science and Engineering: A, 186 (1994) 43-50.
[18] A. Dubinko, D. Terentyev, A. Bakaeva, K. Verbeken, M. Wirtz, M. Hernández-Mayoral, Evolution of plastic deformation in heavily deformed and recrystallized tungsten of ITER specification studied by TEM, International Journal of Refractory Metals and Hard Materials, 66 (2017) 105-115.
[19] J.R. Stephens, Dislocation structures in single-crystal tungsten and tungsten alloys, Metallurgical Transactions, 1 (1970) 1293-1301.
[20] S. Kok, A.J. Beaudoin, D.A. Tortorelli, On the development of stage IV hardening using a model based on the mechanical threshold, Acta Materialia, 50 (2002) 1653-1667.
[21] E.I. Galindo-Nava, P.E.J. Rivera-Díaz-del-Castillo, Modelling plastic deformation in BCC metals: Dynamic recovery and cell formation effects, Materials Science and Engineering: A, 558 (2012) 641-648.
[22] M. Knezevic, I.J. Beyerlein, M.L. Lovato, C.N. Tomé, A.W. Richards, R.J. McCabe, A strain-rate and temperature dependent constitutive model for BCC metals incorporating non-Schmid effects: Application to tantalum-tungsten alloys, International Journal of Plasticity, 62 (2014) 72-92.
[23] H. Sheng, G. Van Oost, E. Zhurkin, D. Terentyev, V.I. Dubinko, I. Uytdenhouwen, J. Vleugels, High temperature strain hardening behavior in double forged and potassium doped tungsten, Journal of Nuclear Materials, 444 (2014) 214-219.
[24] T. Hirai, S. Panayotis, V.R. Barabash, C. Amzallag, F. Escourbiac, A. Durocher, M. Merola, J. Linke, T. Loewenhoff, G. Pintsuk, M. Wirtz, I. Uytdenhouwen, Use of tungsten material for the ITER divertor, Nuclear Materials and Energy, 9 (2016) 616-622.

[25] E. Voce, J Inst Metals, 74 (1968).
[26] Y. Estrin, H. Mecking, A unified phenomenological description of work hardening and creep based on one-parameter models, Acta Metallurgica, 32 (1984) 57-70.
[27] I.J. Beyerlein, C.N. Tomé, A dislocation-based constitutive law for pure Zr including temperature effects, International Journal of Plasticity, 24 (2008) 867-895.
[28] W.F. Hosford, R.M. Caddell, Metal forming. Mechanics and Metallurgy, Cambridge University Press, 2007.
[29] I.S. Yasnikov, A. Vinogradov, Y. Estrin, Revisiting the Considère criterion from the viewpoint of dislocation theory fundamentals, Scripta Materialia, 76 (2014) 37-40.
[30] ASTM Int., ASTM E8/E8M-15a Standard Test Methods for Tension Testing of Metallic Materials, (2015) 1-27.
[31] T.V. Elzhov, K.M. Mullen, A.-N. Spiess, B. Bolker, minpack.lm: R Interface to the Levenberg-Marquardt Nonlinear Least-Squares Algorithm Found in MINPACK, Plus Support for Bounds. R package version 1.2-0. https://CRAN.R-project.org/package=minpack.lm, (2015).
[32] R Core Team, R: A language and environment for statistical computing. R Foundation for Statistical Computing, Vienna, Austria. URL https://www.R-project.org/, (2017).
[33] M. Müller, M. Zehetbauer, A. Borbély, T. Ungár, Stage IV work hardening in cell forming materials, part I: Features of the dislocation structure determined by X-ray line broadening, Scripta Materialia, 35 (1996) 1461-1466.
[34] C. Geuzaine, J.F. Remacle, Gmsh: A 3-D finite element mesh generator with built-in pre- and post-processing facilities, Int J Numer Meth Eng, 79 (2009) 1309-1331.
[35] A.M. Lennon, K.T. Ramesh, The thermoviscoplastic response of polycrystalline tungsten in compression, Materials Science and Engineering: A, 276 (2000) 9-21.
[36] A. Hasegawa, M. Fukuda, S. Nogami, K. Yabuuchi, Neutron irradiation effects on tungsten materials, Fusion Engineering and Design, 89 (2014) 1568-1572.
[37] T. Tanno, A. Hasegawa, J.C. He, M. Fujiwara, M. Satou, S. Nogami, K. Abe, T. Shishido, Effects of transmutation elements on the microstructural evolution and electrical resistivity of neutron-irradiated tungsten, Journal of Nuclear Materials, 386-88 (2009) 218-221.